J Seismol (2016) 20:107–116
DOI 10.1007/s10950-015-9513-0

ORIGINAL ARTICLE

Exploration of deep sedimentary layers in Tacna city, southern Peru, using microtremors and earthquake data for estimation of local amplification

Hiroaki Yamanaka · Mileyvi Selene Quispe Gamero · Kosuke Chimoto · Kouichiro Saguchi · Diana Calderon · Fernándo Lázares La Rosa · Zenón Aguilar Bardales

Received: 9 April 2014 / Accepted: 3 August 2015 / Published online: 13 August 2015

Abstract S-wave velocity profiles of sedimentary layers in Tacna, southern Peru, based on analysis of microtremor array data and earthquake records, have been determined for estimation of site amplification. We investigated vertical component of microtremors in temporary arrays at two sites in the city for Rayleigh wave phase velocity. A receiver function was also estimated from existing earthquake data at a strong motion station near one of the microtremor exploration sites. The phase velocity and the receiver function were jointly inverted to S-wave velocity profiles. The depths to the basement with an S-wave velocity of 2.8 km/s at the two sites are similar as about 1 km. The top soil at the site in a severely damaged area in the city had a lower S-wave velocity than that in a slightly damaged area during the 2001 southern Peru earthquake. We subsequently estimate site amplifications from the velocity profiles and find that amplification is large at periods from 0.2 to 0.8 s at the damaged area indicating possible reasons for the differences in the damage observed during the 2001 southern Peru earthquake.

H. Yamanaka (✉) · M. S. Q. Gamero · K. Chimoto · K. Saguchi
Interdisciplinary Graduate School of Science and Engineering, Tokyo Institute of Technology, 4259 Nagatsuta, Midori-ku, Yokohama, Kanagawa 226-8503, Japan
e-mail: yamanaka@depe.titech.ac.jp

D. Calderon · F. L. La Rosa · Z. A. Bardales
Japan Peru Center for Earthquake Engineering Research and Disaster Mitigation (CISMID), National University of Engineering, Av. Tupac Amaru 1150, Rimac. Lima, Peru

Keywords S-wave profile · Microtremors · Rayleigh wave phase velocity · Receiver function · Site amplification · 2001 southern Peru earthquake

1 Introduction

The 23 June 2001 southern Peru earthquake of M_w 8.4 was a large thrust earthquake on the plate boundary between the Nazca plate and the South American plate with a low dip angle in the north-east direction (e.g., Tavera et al. 2006). The fault area was 320 km by 100 km in length and width, with its epicenter in the north-western end of the fault (Giovanni et al. 2002). The unilateral faulting contains a complex rupture process with variable rupture velocities and a heterogeneous slip distribution (Robinson et al. 2006). Strong shaking was experienced in several major cities in southern Peru during the earthquake. The maximum intensities on the MSK79 scale of 6 to 7 were observed in Arequipa, Moquegua, and Tacna (Tavera et al. 2006). The high intensity area was elongated from the epicenter along the fault plane, because of source directivity effects. Analysis of strong motion records during the main shock suggests that large ground shaking at Moquegua may have been partly caused by directivity effects (Dewey et al. 2003). Since no strong motion records for the earthquake were available at the other damaged cities in southern Peru, ground motion characteristics are still unknown. In Tacna city in southern Peru, old adobe buildings were damaged during the earthquake.

Especially, significant damage to one- or two-story buildings was observed in the northeastern part of Tacna city (Rodriguez-Marek et al. 2003). Tavera et al. (2006) estimated the distribution of seismic intensity in Tacna from the damage observations. Their results clearly indicate that the maximum intensities were as large as 7− on the MSK79 scale in the northeastern part of the city and as low as 6− or 5+ in the southern part. Since the city is located at an epicentral distance of more than 100 km, these differences may be caused by local site conditions in the city together with differences in structural performance (Rodriguez-Marek et al. 2003).

Geotechnical and geophysical investigations were conducted in damaged areas in southern Peru. Rodriguez-Marek et al. (2010) conducted surface wave surveys in Moquegua and revealed S-wave velocity profiles down to a depth of 20 m, whose bottom layer has an S-wave velocity of about 800 m/s. The estimated amplifications at the sites were large in a frequency range higher than 5 Hz; no significant amplifications can be expected at frequencies lower than 5 Hz. They suggested that an average S-wave velocities in the top 30 m may be insufficient to explain the strong ground motion features at periods longer than 1 s at Moquegua due to the lack of amplification of S-waves in deep S-wave velocity layers. Since no field surveys for S-wave profiles have been conducted in Tacna city, the reasons for the site effects in the city remain unknown. However, it is likely necessary to obtain sufficiently deep S-wave velocity profiles down to the basement, as suggested in the investigation of ground motion in Moquegua.

In this study, we conducted microtremor array measurements and an analysis of earthquake ground motion records at Tacna city in order to estimate S-wave velocity profiles. We discuss these profiles in the context of site amplification factors in the city.

2 Observation

Tacna city is located in a valley along the Caplina river which is covered with conglomerate in Quaternary age (Rodriguez-Marek et al. 2003). The valley is bounded by hills of Tertiary age in the northwest and southeast, as can be seen in the topographical map in Fig. 1. Microtremor explorations were conducted at two sites in Tacna as shown in Fig. 1. The TAC site was located in the northern part of the city where structural damage was severe during the 2001 earthquake as can be seen in Fig. 2. UNJB was in an area with lower seismic intensity than that around the TAC station.

Three temporary arrays were deployed at each site. Each array consisted of seven instruments installed as double-triangle shapes, having side lengths of 1.5–3, 6–12, or 24–48 m with a center as shown in Fig. 3. The instruments used included an accelerometer and a recording unit with GPS timing receiver (GPL-6A3P by Mitsutoyo Corp.). The accelerometers used are basically similar to Kudo et al. (2002). Timing of the stations was corrected by the GPS time signal before the measurements to obtain simultaneous records in an array. Vertical microtremor data with durations of 15 to 30 min were acquired with a sampling interval of 0.01 s in each array. Although we conducted array measurements using large arrays with side lengths more than 100 m, we could not obtain microtremor records with sufficiently large amplitudes over noise level at low frequency in such large arrays. Therefore, we used the data from the measurements in the arrays with side lengths less than 48 m.

In this area, earthquake observation using a strong motion instrument has previously been conducted by CISMID (Japan Peru Center for Earthquake Engineering Research and Disaster Mitigation) as shown in Figs. 1 and 2. The station, UPT, is located near the site of UNJB in the southern part of the city corresponding to the low-intensity area. We used three-component data of earthquake records at the station in our analysis.

3 Analysis

3.1 Estimation of phase velocity

The microtremor data in each array were used in spatial autocorrelation (SPAC in the following) analysis (e.g., Okada 2003; Kudo et al. 2002; Roberts and Asten 2005) to retrieve Rayleigh wave phase velocities. In processing the array data, records were divided into segments of 81.92-s duration without large artificial impulsive disturbances. Records from the seven sensors in each segment were converted to Fourier spectra. An example of the array data from TAC is displayed in Fig. 4 along with their spectra. The spectra were very similar at a frequency range higher than 4 Hz. We, next, calculated

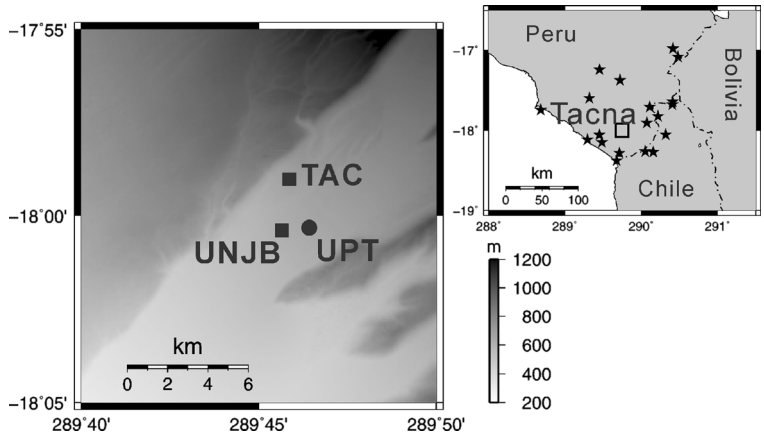

Fig. 1 Location of studies area in Tacna, southern Peru, with surface topography. *Left figure* shows the locations of sites for microtremor array explorations and an earthquake observation station denoted by *squares* and a *circle*, respectively. *Rectangular in the right figure* shows the area for the *left figure*. Stars in the right figure indicate epicenters of earthquakes used in receiver function analysis

SPAC coefficients using the spectra. After we processed all segments, SPAC coefficients were averaged for further processing. Figure 5 shows an example of the SPAC coefficients for data from one of the arrays at TAC. The SPAC coefficient is defined as average of standardized cross correlations between data at center and stations on a circle. It can be approximated by the Bessel function. It should be noted that five SPAC coefficients were obtained from the data in each array since there were five combinations of sensor separation distances. The observed coefficients become high at frequency of 5 Hz and decrease at high frequency. The coefficient, ρ, for a radius, r, at frequency, f, is expressed as

$$\rho(f, r) = J_0(2\pi f r / c(f)),$$

where J_0 is the Bessel function of the first kind of zero order, and $c(f)$ is phase velocity (Okada 2003). The coefficients were fitted to the Bessel function at frequency range from 5 to 30 Hz to estimate the phase velocity.

The phase velocities obtained for the two sites are depicted in Fig. 6. The phase velocities were estimated in a frequency range from 5 to 30 Hz. The phase

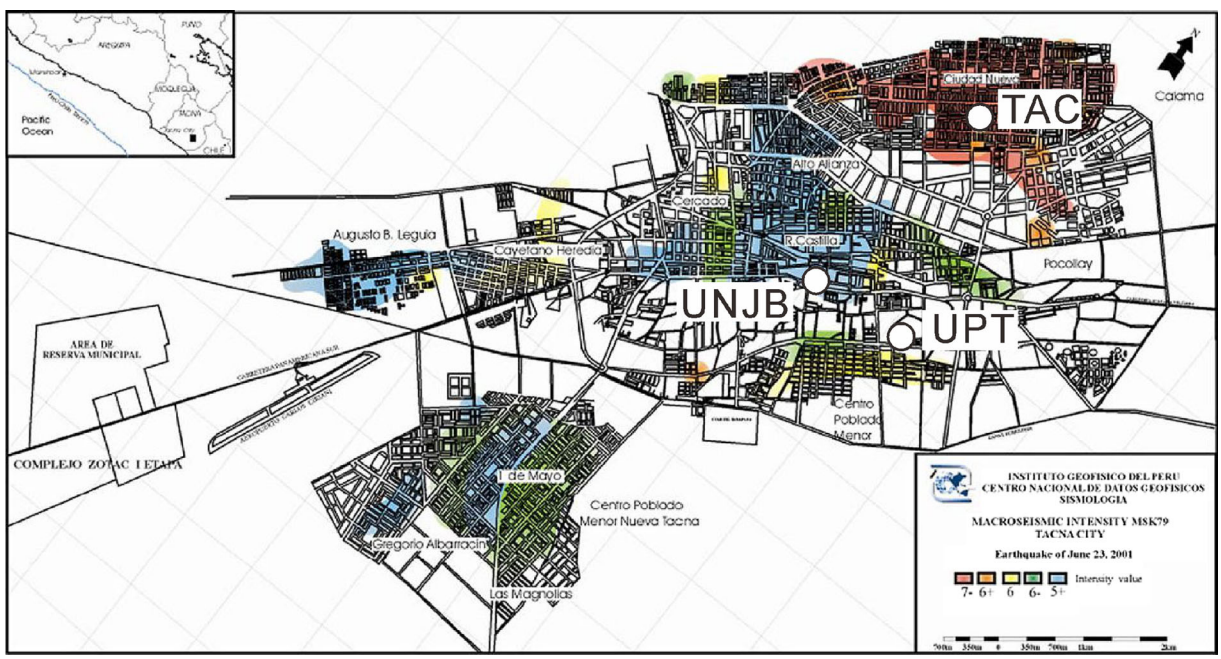

Fig. 2 Map for seismic intensity on MSK79 scale (Tavera et al. 2006) with locations of observation sites in this study

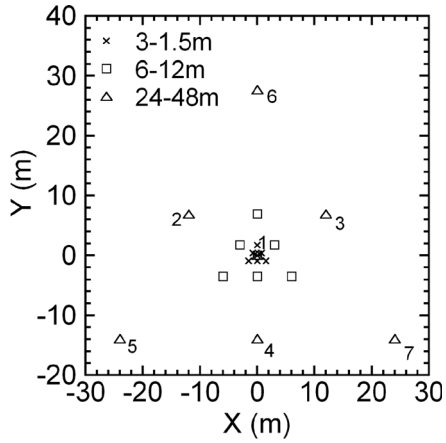

Fig. 3 Array configurations. Three arrays were deployed at each site with seven sensors shown by *crosses*, *squares*, and *triangles*, respectively. Each array is formed in double-triangle shapes with side lengths of 1.5 to 48 m with a center

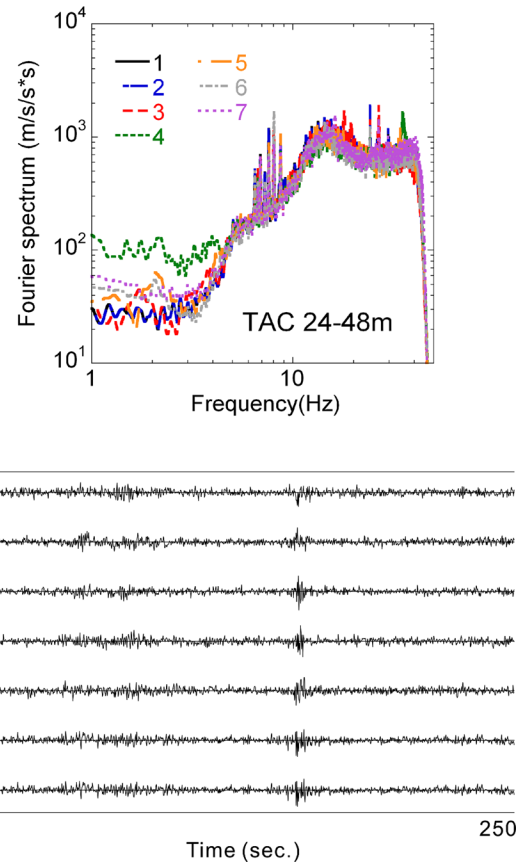

Fig. 4 Observed microtremors and their spectra in array with side lengths of 24 and 48 m at TAC. *Numbers* attached mean station numbers

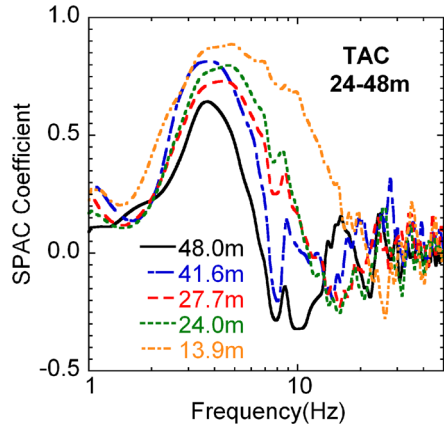

Fig. 5 SPAC coefficients from vertical microtremor data in array with side lengths of 24 and 48 m at TAC

velocity at TAC was lower than that at UNJB across the entire frequency range, indicating the existence of low S-wave velocity layers at TAC. The phase velocity was unfortunately limited at frequencies higher than 5 Hz. It turns out that the lack of the phase velocity at low frequency was due to the low coherency of the microtremor data. This incompleteness of the phase velocity makes it difficult to determine deep S-wave velocity profiles down to the basement from only the phase velocity. Therefore, other data are required to add an additional constraint for deep S-wave profiling.

3.2 Estimation of receiver function

We attempted to use receiver function from earthquake data at the UPT station as an additional constraint. The receiver function method has been widely used in studies on crustal structures using converted S-waves and multiply-reflected P-waves generated by initial P-wave (e.g., Langston 1979).

The earthquake data obtained during 19 events in Table 1 were analyzed for the receiver functions. We selected earthquake records whose P-wave onset could be easily identified. The P-wave portion with duration of 5.12 s with additional taper parts of 1 s was used in the processing for the receiver function. The procedure for data processing in the frequency domain with a water table (e.g., Kurose and Yamanaka 2006) was applied to the P-wave parts. As a first step in the processing, spectra of vertical and radial components in initial P-wave portions were calculated. Examples of the earthquake records are shown in Fig. 7. Then a receiver function was calculated by vertical division of the horizontal spectrum

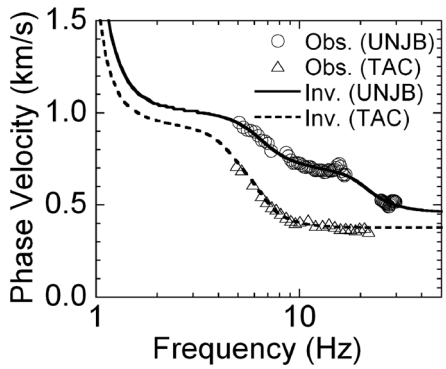

Fig. 6 Comparison of observed phase velocities at UNJB and TAC denoted by *circles* and *triangles* with theoretical ones for fundamental Rayleigh waves in the inverted models shown by *solid* and *broken lines*, respectively

for each event, which was used to obtain averaged one before inverse Fourier transform into the time domain. Figure 8 shows the averaged receiver function. Large phases can be seen within times of 0.6 s.

4 Inversion to S-wave velocity profile

We used the phase velocity at UNJB and the receiver function at UPT jointly in a determination of an S-wave

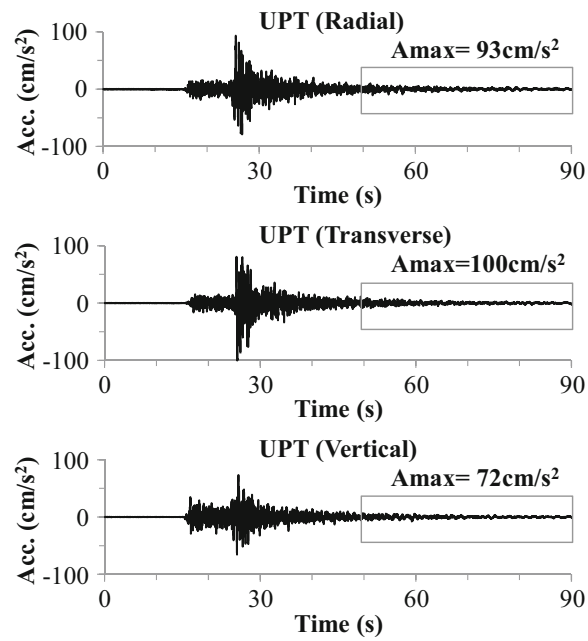

Fig. 7 Example of three components of earthquake records at UPT during the event no. 12. The *rectangular boxes* attached to the records indicate coda part used for calculating horizontal to vertical ratio

Table 1 Earthquake source parameters by USGS

No.	Date	Time	Lat.	Long.	Depth (km)	*M*
1	2003/10/26	11:27	−17.708	−69.887	108	5.3
2	2004/05/30	11:45	−17.243	−70.546	109	5.5
3	2004/07/23	07:14	−18.284	−70.285	114	4.6
4	2004/08/05	08:23	−18.271	−69.842	28	4.3
5	2004/11/01	22:51	−18.379	−70.321	43	5.0
6	2004/11/11	04:12	−16.978	−69.583	144	5.4
7	2009/03/30	10:48	−17.907	−69.925	99	4.5
8	2009/06/13	15:11	−17.746	−71.317	43	5.3
9	2009/09/22	13:32	−17.597	−70.680	75	4.2
10	2010/01/17	07:15	−18.265	−69.946	99	4.3
11	2010/04/23	20:17	−18.056	−69.678	124	4.6
12	2010/05/05	21:42	−18.058	−70.547	37	6.2
13	2010/05/05	21:58	−18.151	−70.514	35	4.1
14	2010/05/06	01:32	−18.117	−70.704	56	4.6
15	2010/08/04	23:53	−17.373	−70.278	104	4.7
16	2011/06/07	22:06	−17.083	−69.518	146	5.9
17	2011/06/18	00:38	−17.641	−69.587	112	4.8
18	2012/05/14	05:01	−17.678	−69.591	106	6.2
19	2012/06/11	18:38	−17.824	−69.780	94	4.9

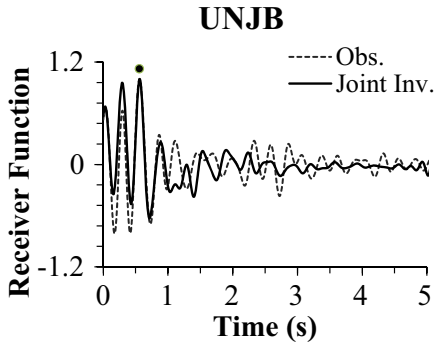

Fig. 8 Receiver functions observed and calculated from inverted model at UNJB in Fig. 10 shown by *solid* and *broken lines*, respectively

velocity profile considering the incomplete frequency range of the observed phase velocity. The misfit in the joint inversion (Julia et al. 2002) is defined as

$$\phi = p\phi_{PH} + (1-p)\phi_{RF}$$

using the misfits for the phase velocity, ϕ_{PH}, and receiver function, ϕ_{RF}, with a weight of p. According to Kurose and Yamanaka (2006), p was set to be 0.5. Each misfit was calculated from

$$\phi_{PH} = \frac{1}{N}\sum_{i=1}^{N}\left(\frac{C_i^C - C_i^O}{C_i^O}\right)^2,$$

and

$$\phi_{RF} = \frac{1}{M}\sum_{j=1}^{M}\left(\frac{R_j^C - R_j^O}{R_j^O}\right)^2.$$

Here, C_i^C and C_i^O are the calculated and the observed phase velocities at N frequencies, while and R_j^C are R_j^O are the calculated and the observed receiver functions at M time steps. This misfit was minimized with simulated annealing (e.g., Yamanaka 2005) for finding P-wave velocity, S-wave velocity, and thickness of the best layered model. Densities were given in advance. The search limits of the parameters are tabulated in Table 2. We assumed narrow search limits for S-wave velocity to avoid velocity-inverse layer, while relatively wide limits are used for thickness.

The results of the inversion at UNJB are shown in Fig. 9 and in Table 3. The top layer had an S-wave velocity of 400 m/s with a thickness of 10 m indicating a very stiff site condition. The basement, having an S-wave velocity of 2.8 km/s, was located at a depth of about 1 km. In order to understand the uncertainty of the S-wave velocity model at UNJB, all the acceptable models are compared. The acceptable model is defined as model whose misfit is less than 1.1 times of the minimum misfit value. All the acceptable models in Fig. 9 are similar indicating an appropriateness of the inverted model. The evolutions of current and minimum misfits are also shown in the figure. The misfit decreases rapidly within the first 4000 iterations. Comparison between the observations and the synthetics for the inverted model can be seen in Fig. 8 for the receiver function and in Fig. 6 for the phase velocity. The phase velocity was reproduced well by the inverted model. The major phases at arrival times shorter than 1.0 s in the receiver function were also sufficiently explained with the theoretical one.

Here, we calculated the ratio of the horizontal and vertical spectrums for the coda part of the earthquake records at UPT near UNJB. An example of the coda part used is displayed in Fig. 7. After the horizontal to vertical ratio for each event was calculated, they were averaged in the data processing. This ratio has often been used in validation of S-wave velocity models, interpreted as Rayleigh wave ellipticity (e.g., Yamanaka et al. 1994). Figure 11 compares the observed horizontal to vertical ratio with the theoretical ellipticity for fundamental and four higher modes of Rayleigh waves in the model of UNJB. Although the observed peak value was slightly smaller than the theoretical one, the peak period of the observed ratio at a period of 0.3 s agrees well with the theoretical solution, indicating an appropriate velocity model at UNJB.

Table 2 Search limits in joint inversion of phase velocity and receiver function observed at UNJB

Layer	ρ (kg/m^3)	*Vp* (m/s)	*Vs* (m/s)	*Qp*	*Qs*	*H* (m)
1	1800	1500–1800	200–500	120	70	1–50
2	2000	1800–2400	500–1000	200	120	20–100
3	2150	2400–3000	1000–1500	340	200	200–500
4	2300	3000–4200	1500–2500	580	350	300–600
5	2600	4400–5000	2500–3200	680	400	∞

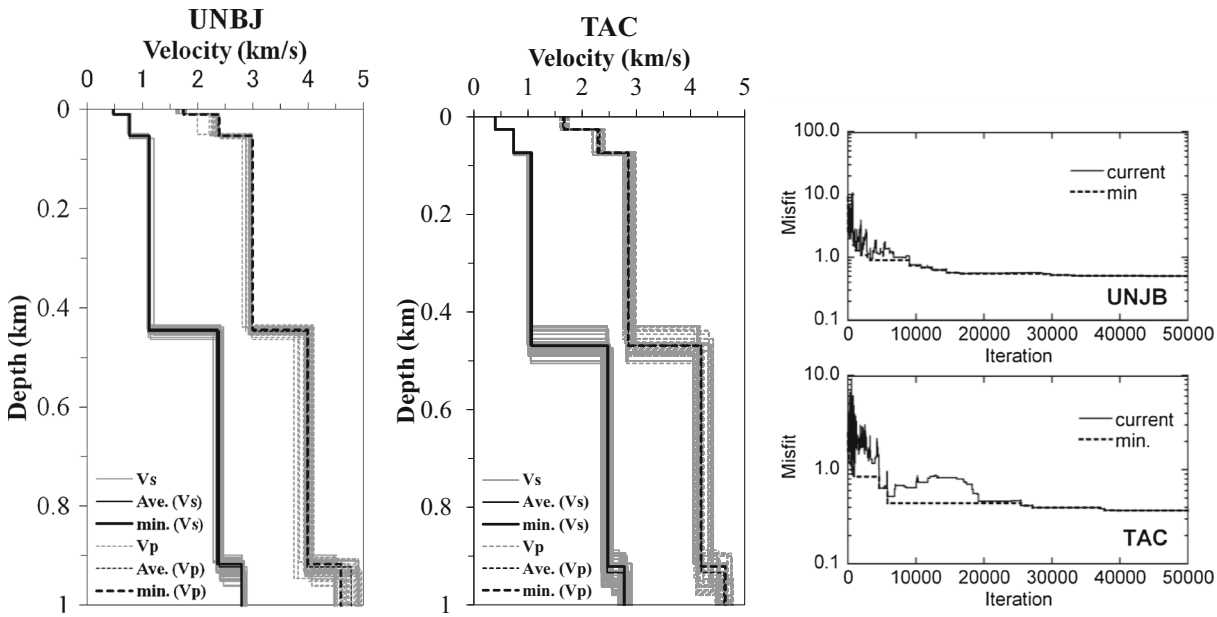

Fig. 9 Results of inversion of phase velocity and receiver function. *Left* and *central panels* indicate S-wave velocity profiles at UNJB and TAC. *Black* and *gray lines* show optimal model and models whose misfits are less than 1.1 times of the minimum misfit value, respectively. *Right panel* shows variations of the minimum and current misfits against number of iterations in the inversions

We next determined an S-wave velocity profile beneath the TAC station from only the phase velocity by taking into account the results of the above joint inversion for UNJB. Since the phase velocity at TAC was also limited at high frequencies, we defined narrow search limits of the parameters in the inversion of the phase velocity as shown in Table 4. The search areas for the parameters of the deep part of the profile were set to be as narrow as 5 % of the parameters derived in the joint inversion for UNJB, while those for the shallow part were relatively wide. The profile from the inversion of the phase velocity at TAC is shown in Fig. 9. All the acceptable models are similar to the optimal model indicating appropriateness of the inverted model. Comparison of the observed and calculated phase velocities at TAC indicates good agreement as shown in Fig. 6. Figure 10 compares the S-wave profiles at the two sites. The deep part of the profile at TAC was almost

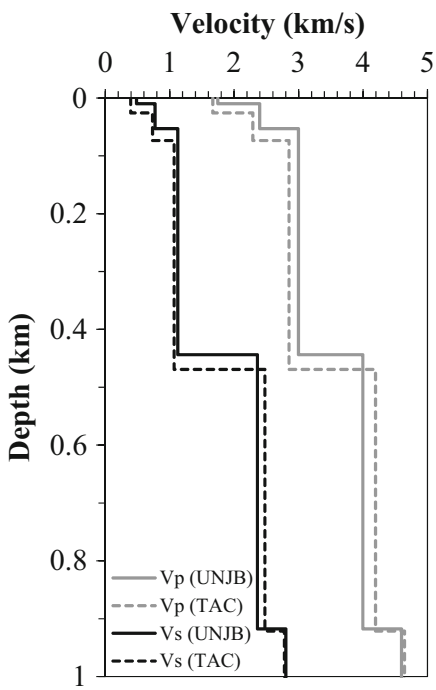

Fig. 10 Comparison of S-wave and P-wave velocity profiles at UNJB and TAC

Table 3 Subsurface structural model from inversion

Layer	TAC			UNJB		
	Vp (m/s)	*Vs* (m/s)	*H* (m)	*Vp* (m/s)	*Vs* (m/s)	*H* (m)
1	1670	400	26	1745	490	10
2	2290	735	48	2395	775	45
3	2850	1070	395	3000	1125	390
4	4195	2475	450	4000	2360	475
5	4645	2780	–	4595	2800	–

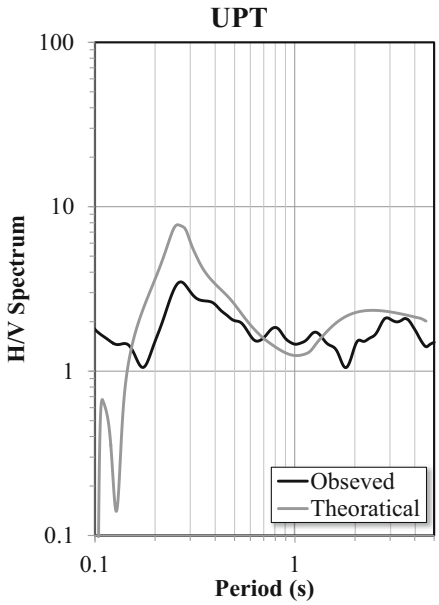

Fig. 11 Horizontal to vertical ratio of coda waves in earthquake records. Observed ratio and theoretical ellipticity for fundamental and four higher modes of Rayleigh waves in inverted model at UNJB in Fig. 10 are shown by *black* and *gray lines*, respectively

the same as that of UNJB. However, the top layer at TAC was lower in S-wave velocity and thicker than that of UNJB.

5 Discussion

The inverted results indicate the existence of a thicker top layer with a low S-wave velocity of 400 m/s at TAC compared to the area around UNJB. Here, we compare the amplification factors for the two inverted models. A 1D reverberation theory of vertical propagating S-waves in a homogeneous layered model was used in calculating amplifications. Constant Q-value was assumed to be 1/5 of S-wave velocity in m/s. The 1D amplification factors of S-wave for the two sites are displayed in

Table 4 Search limits in inversion of phase velocity at TAC

Layer	*Vp* (m/s)	*Vs* (m/s)	*H* (m)
1	±20 % of UNJB	±20 % of UNJB	1–50
2	±5 % of UNJB	±5 % of UNJB	10–200
3	±5 % of UNJB	±5 % of UNJB	±10 % of UNJB
4	±5 % of UNJB	±5 % of UNJB	±10 % of UNJB
5	±5 % of UNJB	±5 % of UNJB	∞

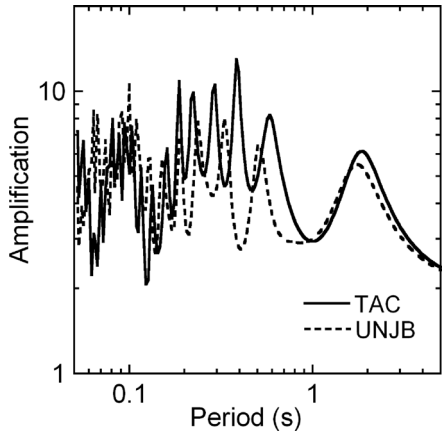

Fig. 12 Amplification factors for S-waves in inverted models at TAC and UNJB

Fig. 12. The two sites had a similar peak at a period of 2 s. However, the amplitude at TAC was larger on average than UNJB in the period range 0.2 to 0.8 s. This difference qualitatively suggests one of the possible reasons for the higher damage in TAC than UNJB during the 2001 southern Peru earthquake.

We further investigated the amplification factors at TAC. We calculated 1D amplification factors using three models modified from the inverted profile at TAC. The first model (M1-4) was generated by neglecting the fifth layer, having an S-wave velocity of about 2.8 km/s in the original model (M1-5) having five layers. The bottom two layers in the inverted model were replaced with the third layer with an S-wave velocity of 1.1 km/s in the second modified model (M1-3). In the last model (M1-2), the bottom three layers were modified to have the same velocity as the second layer,

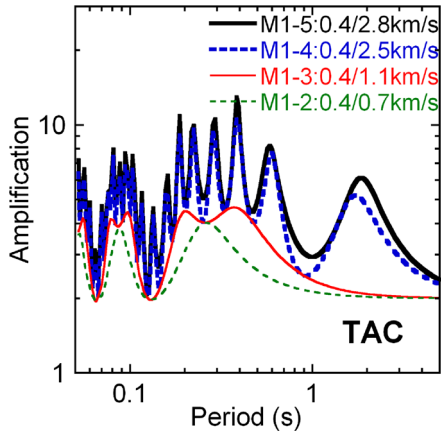

Fig. 13 Amplification factors of S-waves in inverted model (M1-5) and modified models by neglecting deep layers (M1-4 to M1-2)

with an S-wave velocity of 0.7 km/s. The M1-2 model can be regarded as shallow soil model without any deep layers. The amplifications for the modified models were compared with that of the original inverted model in Fig. 13. The model M1-4 has a similar amplification to that of the original inverted model (M1-5) at entire period range. This indicates the importance of the top three layers over the layer having an S-wave velocity of 2.5 km/s in the characterization of site effects. The models M1-2 and M1-3 show the amplifications with peaks at 0.2 to 0.4 s indicating the effects of the shallow soil over the layer with an S-wave velocity of 1.1 km/s. However, the original model (M1-5) also contains several larger peaks in the amplifications at periods shorter than 0.4 s. Furthermore, additional peak at periods longer than 0.6 s cannot be explained with the shallow models of M1-2 and M1-3. Considering these comparisons, the effects due to the deep sediments over the layer with an S-wave velocity of 2.5 km/s are necessary for estimating short-period ground motion in the area. This can be also important in understanding the distribution of earthquake damage during the 2001 southern Peru earthquake.

6 Conclusions

Microtremor array explorations were conducted at the two sites in Tacna, southern Peru, to understand S-wave velocity distributions in deep sedimentary layers. Rayleigh wave phase velocities were estimated from SPAC analysis of the arrays records of vertical microtremors at a frequency range from 5 to 30 Hz. We also obtained the receiver function from earthquake data near one of the microtremor sites. The phase velocity and the receiver function were jointly inverted to an S-wave velocity profiles down to the basement at a depth of about 1 km at the sites. The two sites have no shallow soft soil with an S-wave velocity less than 0.3 km/s. The S-wave velocity profile in the high-intensity area during the 2001 southern Peru earthquake was mainly characterized by the top thicker layer with lower S-wave velocity than that in the low-intensity area. The effects of the different S-wave profiles were evaluated through 1D amplifications of S-waves. Comparison of the amplifications indicates that the amplitudes in a period range from 0.2 to 0.8 s are large in the high-intensity area in the city. This difference suggests one of the possible reasons for the distribution of damage in Tacna during the 2001 earthquake.

Acknowledgments We thank Dina Cotrado Flores, Private University of Tacna, for her support and discussion. We also appreciate students at National University of Engineering and Private University of Tacna for their support in microtremor measurements. We also thank two anonymous reviewers for comments to improve the manuscript. This study was supported with the JST-JICA SATREPS project, "Enhancement of Earthquake and Tsunami Disaster Mitigation Technology in Peru."

References

Dewey JW, Silva WJ, Tavera H (2003) Seismicity and tectonics. Earthquake Spectra 19(S1):1–10. doi:10.1193/1.1737245

Giovanni MK, Beck SL, Wagner L (2002) The June 23, 2001 Peru earthquake and the southern Peru subduction zone. Geophys Res Lett 29:2018. doi:10.1029/2002GL015774

Julia J, Ammon CJ, Herrmann RB, Correig AM (2002) Joint inversion of receiver function and surface wave dispersion observations. Geophys J Int 143:99–112

Kudo K, Kanno T, Okada H, Ozel O, Erdik M, Sasatani T, Higashi S, Takahashi M, Yoshida K (2002) Site specific issues for strong ground motions during the Kocaeli, Turkey earthquake of August 17, 1999, as inferred from array observations of microtremors and aftershocks. Bull Seismol Soc Am 92:448–465

Kurose T, Yamanaka H (2006) Joint inversion of receiver function and surface-wave phase velocity for estimation of shear-wave velocity of sedimentary layers. Explor Geophys 37: 93–101

Langston CA (1979) Structure under Mount Rainier, Washington, inferred from teleseismic bodywaves. J Geophys Res 84: 4749–4762

Okada H (2003) The microtremor survey method: Soc. Exp. Geophy., Tulsa, OK

Roberts J, Asten M (2005) Estimating the shear velocity profile of Quaternary silts using microtremor array (SPAC) measurements. Explor Geophys 36:34–40

Robinson DP, Das S, Watts AB (2006) Earthquake rupture stalled by a subducting fracture zone. Science 312:1203. doi:10.1126/science.1125771

Rodriguez-Marek A, Williams JL, Repetto PC, Rondinel E, Zegarra-Pellane J, Baures DM (2003) Ground motion and site response. Earthquake Spectra 19(S1):11–34. doi:10.1193/1.1737246

Rodriguez-Marek A, Bay JA, Park K, Montalva GA, Cortez-Flores A, Wartman J, Boroschekg R (2010) Engineering analysis of ground motion records from the 2001 Mw 8.4 Southern Peru earthquake. Earthquake Spectra 26(2): 499–524

Tavera H, Fernández E, Bernal I, Antayhua Y, Agüero C, Salas H, Rodríguez S, Vilcapoma L, Zamudio Y, Portugal D, Inza A, Carpio J, Ccallo F, Valdivia I (2006) The southern region of Peru earthquake of June 23rd, 2001. J Seismol. doi:10.1007/s10950-006-9014-2

Yamanaka H (2005) Comparison of performance of heuristic search methods for phase velocity inversion in shallow surface wave method. J Environ Eng Geophys 10: 163–173

Yamanaka H, Takemura M, Ishida H, Niwa M (1994) Characteristics of long-period microtremors and their applicability in exploration of deep sedimentary layers. Bull Seismol Soc Am 84: 1831–1841